Phase transitions in diblock copolymers: Theory and Monte Carlo simulations

Andrea Weyersberg and Thomas A. Vilgis
Max-Planck-Institut für Polymerforschung, P.O. Box 3148, D-55021 Mainz, Germany
(Received 23 November 1992)

The ordering phenomena of symmetric diblock copolymers at the microphase separation transition (MST) are studied both by Monte Carlo simulations using the cooperative-motion algorithm for dense polymer systems in three dimensions and analytically by the random-phase approximation (RPA) applying the Edwards Hamiltonian approach. The transition temperature is found from an analysis of the specific heat of the copolymer melt. Besides a phase separation into a definite lamellar structure, a stretching of the chains and an ordering effect at the MST are observed in the simulations. The RPA is able to explain this elongation of the chains. Additionally, the influence of vacancies on the location of the MST and the static properties of the chains are analyzed by theory and simulations. The vacancies are found to make the melt compatible and to lower the critical temperature.

PACS number(s): 05.70.Fh, 05.40.+j, 61.41.+e, 36.20.−r

I. INTRODUCTION

The investigation of block copolymers is a very recent field of polymer science. Interesting applications of diblock copolymers in material science make this field a matter of interest in experiments [1–8], theory [9–16], and computer simulations [17–19].

A pioneering work in the theory of the weak segregation limit (small interaction parameters $\chi_F N$ only) was presented by Leibler in 1980 [20]. This theory uses the random-phase approximation (RPA) in a macroscopic version of the Landau theory. The predictions of this theory could qualitatively explain the experimental findings on diblock copolymers. Such results concern the periodic structure which arises in experimental situations, i.e., for a given composition, and the critical temperature. A more advanced analysis by Fredrickson and Helfand [10] included the fluctuations of the order-parameter correlation in the well-known Brazovskii approximation [21] and gave a description of the structures of asymmetric diblock copolymers which is in better agreement with experiments. A correction to the critical temperature, which is inversely proportional to the degree of polymerization N, was also found. Common Monte Carlo lattice algorithms for the simulation of polymer melts use a certain amount of vacancies to relax the ensembles of configurations, in order to respect the excluded volume constraint [17–19,22–24]. To our knowledge there are two algorithms presented in the literature which are capable of simulating dense polymer melts: the bond-breaking algorithm [25] and the cooperative-motion algorithm (CMA) [26–30]. Only the latter can simulate well-defined monodisperse polymers in the static limit. In the following sections we investigated the thermodynamic behavior of symmetric diblock copolymers by simulation using the cooperative-motion algorithm. This represents the first time, to our knowledge, monodisperse diblock copolymer melts in the limit of density $\phi=1$ have been simulated on a lattice. We also study the influence of vacancies on static properties and on the critical behavior. The paper is organized as follows. The following section describes the cooperative-motion algorithm. In a theoretical section the basic equations for block copolymers are presented; expressions for structure factors and effective interaction potentials between arbitrary monomers are given. These mean-field predictions are analyzed with respect to the numerical data presented in Sec. IV. It is demonstrated that the mean-field predictions can be verified very well. The RPA is then extended to the case where vacancies are important. The stability limit and the effective potentials depend strongly on the vacancy concentration. These results are also compared to simulation data, in which the vacancy concentration is varied.

II. THE COOPERATIVE MOTION ALGORITHM

The cooperative-motion algorithm allows one to simulate polymer melts at a density $\phi=1$ on a lattice [26–30]. The lattice is completely occupied by monomers and the monomers of each chain are connected by $(N-1)$ bonds of constant length a. To take into account excluded volume effects we restrict the chain configurations to *self-avoiding* and *mutually avoiding* walks. In the case of diblock copolymers two chains of either monomer type A or type B are connected to form the copolymer with length $N=N_A+N_B$. The two types of monomer are partially compatible and we introduce interaction parameters ε_{ij}, where the choice $\varepsilon_{AA}=\varepsilon_{BB}=0$ and $\varepsilon_{AB}=\varepsilon=1$ is taken without loss of generality. Each monomer can therefore be labeled by a spin variable $\sigma=+1,-1$. The energy of one monomer is the sum over all q nearest neighbors which have a different spin variable; in the case of an A monomer the sum is taken over all B monomers out of q next neighbors, $E(A)=\sum_{B\in(q)}\varepsilon_{AB}$. The nature of the algorithm is *cooperative*, as in dense systems ($\phi=1$) a segment of one chain can only be moved by simultaneously moving other segments of different chains [see the dashed bonds and the monomers (squares) of Fig. 1(b) in comparison to Fig. 1(a)]. In another paper [30] the tech-

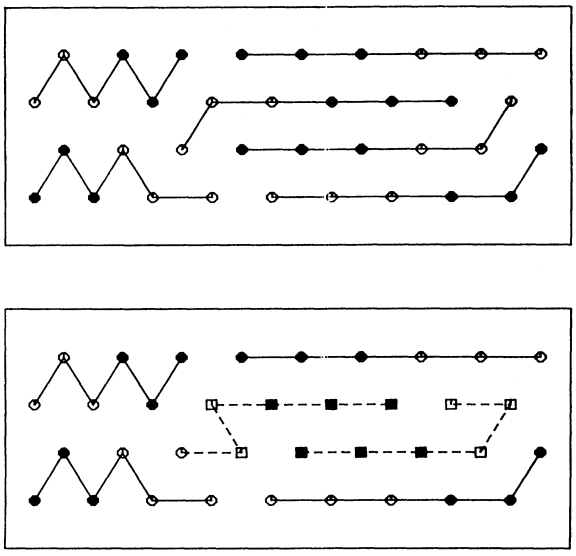

FIG. 1. (a) Configuration of a copolymer melt. The white and the black circles characterize the different types of monomers. (b) New configuration of a copolymer melt. The squares characterize the monomers that have been moved, while the dashed lines represent the moved bonds.

nical realization of the algorithm for generating to static properties of different polymer systems is described. To summarize, we mention that we always move chain elements consisting of several monomers as a whole. How it is handled in practice is described in detail in [30]. Moving a chain element alters the local energy because the monomers contact new neighbors. We identify the attempt to move a chain element as one Monte Carlo step, which has been proven to be sensible in the CMA. We now use the common Metropolis test [31] for importance sampling by looking at the energy difference $\Delta E(\text{element})=E_{\text{final}}-E_{\text{initial}}$ for the whole chain element, which as been reorientated. At a given temperature T, the Boltzmann factor $p=\exp[-\Delta E(\text{element})/k_BT]$ is compared with a random number r, $0\le r<1$. If $p\ge r$, the new configuration has been accepted and another chain element will be reorientated. Finally several chains have found a new configuration [Fig. 1(b)] and at this stage we calculate thermodynamic equilibrium quantities. With this procedure of implementing energetic interactions in the algorithm, it is guaranteed that the principle of detailed balance is fulfilled. For the case of codimers the algorithm has been shown to be ergodic [32].

The following results are obtained by simulations on a fcc lattice, where the bonds have the length $a=\sqrt{2}$. The possible bond angles are $\alpha=60°$, 90°, 120°, and 180° with degeneracy $d_\alpha=4,2,4,1$. Every monomer has $q=12$ nearest neighbors in the simulation. We use a lattice of size $L^3=20^3$ containing 4000 monomers, and vary the chain length $N=20,32,50$ and extend these simulations for some temperatures to chain lengths $N=100$. To reduce boundary effects, the usual periodic boundary conditions have been employed.

III. THEORY—DENSE MULTICOMPONENT MELT

The crucial point of this section is to present a partition function (or a generating functional) from which collective and single chain properties can be calculated simultaneously. These quantities will be required to interpret the results of the simulation using the CMA. The method goes back to Edwards and Muthukumar [33] and has been used by Ohta and Nakanishi [34] for semidilute polymer solutions. It is outlined here for multicomponent systems including blends and diblock copolymers. Indeed, as it will become obvious later, the method applies also for more general situations.

We start from the Edwards Hamiltonian for a z-component polymer system

$$\beta\mathcal{H}=\sum_{\sigma=1}^{z}\sum_{\alpha=1}^{\nu^\sigma}\int_0^{N^\sigma}ds\left[\frac{\partial\mathbf{R}_\alpha^\sigma(s)}{\partial s}\right]^2+\sum_{\sigma,\tau=1}^{z}\sum_{\alpha=1}^{\nu^\sigma}\sum_{\beta=1}^{\nu^\tau}\int_0^{N^\sigma}\int_0^{N^\tau}ds\,ds'\times V^{\sigma\tau}[\mathbf{R}_\alpha^\sigma(s)-\mathbf{R}_\beta^\tau(s')]\ . \tag{1}$$

The first term is the Wiener measure, where it has been assumed that the unperturbed chains are Gaussian and the second term represents the binary interactions between two chain segments $\mathbf{R}_\alpha^\sigma(s)$ and $\mathbf{R}_\beta^\tau(s')$ belonging to chains α,β of type σ,τ. The contour variable s ranges from 0 to N^σ,N^τ, respectively. There are ν^σ (ν^τ) chains of type σ (τ) per unit volume, and their degree of polymerization is N^σ (N^τ). For block copolymer melts Eq. (1) holds also, since it can be reformulated more conveniently if in (1) the mixed interaction term is written as

$$\sum_{\alpha,\beta}\int_0^{fN}ds\int_{fN}^{N}ds'V_{AB}[\mathbf{R}_\alpha^A(s)-\mathbf{R}_\beta^B(s')]\ , \tag{2}$$

where fN is the fraction of A monomers and $(1-f)N$ the fraction of B monomers within one copolymer. Moreover, z is set equal to 2. The partition function of the system is defined as the functional integral

$$Z=\int\prod_{\sigma,\alpha,s}\mathcal{D}\mathbf{R}(s)e^{-\beta\mathcal{H}(\{\mathbf{R}_\alpha^\sigma(s)\})}\ . \tag{3}$$

The quantities which are experimentally available are structure factors defined as

$$S^{\sigma\tau}(\mathbf{k})=\left\langle\sum_{\alpha,\beta}\int_0^{N^\sigma}\int_0^{N^\tau}ds\,ds'e^{i\mathbf{k}\cdot[\mathbf{R}_\alpha^\sigma(s)-\mathbf{R}_\beta^\tau(s')]}\right\rangle\ , \tag{4}$$

which describe the composition and density correlations in the systems. The average $\langle\ \rangle$ has to be taken via the Boltzmann factor $e^{-\beta\mathcal{H}}$. To reformulate (3) into a more convenient form, density variables are introduced and the partition function can be rewritten by using the identities

$$1=\int\prod_{\sigma,\mathbf{k}}\mathcal{D}\rho_\mathbf{k}^\sigma\prod_{\mathbf{k},\sigma}\delta\left[\rho_\mathbf{k}^\sigma-\sum_{\alpha=1}^{\nu^\sigma}\int_0^{N^\sigma}e^{i\mathbf{k}\cdot\mathbf{R}_\alpha^\sigma(s)}\right]\ . \tag{5}$$

Simultaneously the functional δ functions can be represented by auxiliary Edwards random fields $\Phi(\mathbf{r})$, i.e.,

$$\prod_\mathbf{k}\delta(\rho_\mathbf{k}^\sigma)\equiv\int\mathcal{D}\Phi_\mathbf{k}^\sigma\exp\left[i\sum_\mathbf{k}\Phi_\mathbf{k}^\sigma\rho_{-\mathbf{k}}^\sigma\right]\ . \tag{6}$$

Some algebra leads to the partition function Z,

$$Z=\int \mathcal{D}\mathbf{R}\mathcal{D}\rho_{\mathbf{k}}\mathcal{D}\Phi_{\mathbf{k}} e^{-\beta\mathcal{H}([\mathbf{R}],[\rho],[\Phi])} , \tag{7}$$

with a Hamiltonian

$$\beta\mathcal{H}=\sum_{\sigma=1}^{z}\sum_{\alpha=1}^{\nu^{\alpha}}\left\{\int_0^{N^\sigma} ds\left[\frac{\partial \mathbf{R}_\alpha^\sigma}{\partial s}\right]^2+i\int_0^{N^\sigma} ds\,\Phi^\sigma(\mathbf{R}_\alpha^\sigma(s))\right\}$$
$$+\sum_{\mathbf{k}} V_{\mathbf{k}}^{\sigma\tau}\rho_{\mathbf{k}}^\sigma\rho_{-\mathbf{k}}^\tau-i\sum_{\mathbf{k}}\Phi_{\mathbf{k}}^\sigma\rho_{-\mathbf{k}}^\sigma . \tag{8}$$

The first term is the Wiener measure and the second term is the interaction of the polymer (σ,α) with an external random field. The advantage of Eq. (8) is that the binary interactions between all monomers of all species have been decoupled. These two terms represent nothing but the partition function of chains in a complex random field, as we will see below. The last two terms are the excluded volume energy and the coupling of the auxiliary fields $\Phi(\mathbf{r})$ with the density fluctuations. Carrying out the ρ-integrals we are left with a generalization of the standard Edwards transformation here generalized to arbitrary multicomponent systems. Equations (7) and (3) are now exactly identical and some useful exact identities can be calculated as has been noted by Oono [35] and later applied in [36].

It is interesting to realize the important advantage of Eq. (8), which is that the originally coupled integration over the $\mathbf{R}_\alpha^\sigma(s)$ variables has been decoupled to single chain contributions only, since the $\mathbf{R}$ part is determined by the identity

$$\prod_{\alpha,\sigma}\left\{\int \mathcal{D}\mathbf{R}_\alpha^\sigma(s)\exp\left[-\int_0^{N^\sigma} ds\left[\frac{\partial \mathbf{R}_\alpha^\sigma}{\partial s}\right]^2-i\int_0^{N^\sigma} ds\,\Phi(\mathbf{R}_\alpha^\sigma(s))\right]\right\}\equiv\prod_{\alpha,\sigma}\int\int d\mathbf{r}\,d\mathbf{r}'G^\sigma(\mathbf{r},\mathbf{r}',N^\sigma,[\Phi^\sigma]) , \tag{9}$$

where the Green functions $G(\mathbf{r},\mathbf{r}',N,[\Phi^\sigma])$ satisfy the standard differential equation

$$\left[\frac{\partial}{\partial N}-\nabla^2+i\Phi(\mathbf{r})\right]G(\mathbf{r},\mathbf{r}',N,[\Phi^\sigma])=\delta(\mathbf{r}-\mathbf{r}')\delta(N) , \tag{10}$$

which describes a polymer in an external random potential. For one-component excluded volume chains this has been analyzed in detail by Edwards [37] and later by Emery [38] and Freed and Kholodenko [39]. From Eqs. (8)–(10) the standard model for the φ^4 theory for dilute homopolymer solutions can be calculated very easily [40,41]. Consequences of this for dilute diblock copolymers will be discussed separately.

The integrals over the Green functions can be exponentiated and the Hamiltonian has the following form, as given by Ohta and Nakanishi [34] for solutions:

$$\mathcal{H}=\sum_{\mathbf{k}}\boldsymbol{\rho}\underline{V}\boldsymbol{\rho}-i\Phi\boldsymbol{\rho}$$
$$+\sum_{\sigma}\nu^\sigma\ln\int\int d\mathbf{r}\,d\mathbf{r}'G^\sigma(\mathbf{r},\mathbf{r}',N^\sigma,[\Phi^\sigma]) , \tag{11}$$

where

$$\underline{V}(\mathbf{k})=\begin{bmatrix} V_{11} & V_{12} & \cdots & V_{1z} \\ V_{21} & V_{22} & \cdots & V_{2z} \\ \cdots & \cdots & \ddots & \cdots \\ V_{z1} & V_{z2} & \cdots & V_{zz} \end{bmatrix} , \tag{12}$$

$$\boldsymbol{\Phi}=(\Phi_1,\Phi_2,\ldots,\Phi_z) , \tag{13}$$

$$\boldsymbol{\rho}=(\rho_1,\rho_2,\ldots,\rho_z) . \tag{14}$$

The last term of Eq. (11) can be expanded in terms of higher-order vertex functions [20,36]. For the purpose of the present paper it will be enough to approximate $\ln\int\int d\mathbf{r}\,d\mathbf{r}'G(\mathbf{r},\mathbf{r}',N^\sigma,[\Phi^\sigma])$ by the lowest order, which corresponds to the second-moment approximation of Eq. (9), i.e.,

$$\prod\int\mathcal{D}\mathbf{R}_\alpha^\sigma(s)\exp\left[-\int_0^{N^\sigma} ds\left[\frac{\partial \mathbf{R}(s)}{\partial s}\right]^2-i\int_0^{N^\sigma} ds\,\Phi(\mathbf{R}_\alpha^\sigma(s))\right]\simeq\exp\left[-\sum_{\sigma,\tau}\sum_{\alpha,\beta}\int_0^{N^\sigma} ds\int_0^{N^\tau} ds'\langle\Phi(\mathbf{R}_\alpha^\sigma(s))\Phi(\mathbf{R}_\beta^\tau(s'))\rangle_0\right] , \tag{15}$$

noting that $\langle\Phi\rangle_0=0$, where

$$\langle x\rangle_0=\int\prod\mathcal{D}\mathbf{R}x\exp\left[-\sum_{\alpha,\sigma}\int_0^{N^\sigma} ds\left[\frac{\partial \mathbf{R}_\alpha^\sigma(s)}{\partial s}\right]^2\right] . \tag{16}$$

This leads directly to the RPA formulation since

$$\langle\Phi\Phi\rangle_0=\sum_{\mathbf{k}}\Phi_{\mathbf{k}}\Phi_{-\mathbf{k}}S_{\sigma\tau}^0(\mathbf{k}) , \tag{17}$$

yielding the effective Gaussian Hamiltonian in statistical mechanics,

$$\beta\mathcal{H}=\sum_{\mathbf{k}}\Phi_{\mathbf{k}}\underline{S}^{0}_{\mathbf{k}}\Phi_{-\mathbf{k}}+\rho_{\mathbf{k}}\underline{V}_{\mathbf{k}}\rho_{-\mathbf{k}}-i\Phi_{\mathbf{k}}\rho_{-\mathbf{k}}\ . \tag{18}$$

The correlation functions $\langle\rho^{\sigma}_{\mathbf{k}}\rho^{\tau}_{-\mathbf{k}}\rangle$ and $\langle\Phi^{\sigma}_{\mathbf{k}}\Phi^{\tau}_{-\mathbf{k}}\rangle$ describe now the structure factors and the effective potentials, respectively, i.e., Benoit's equations

$$\underline{S}(\mathbf{k})=(\underline{S}^{0-1}+\underline{V})^{-1} \tag{19}$$

and

$$\underline{U}^{\text{eff}}(\mathbf{k})=(\underline{S}^{0}+\underline{V}^{-1})^{-1} \tag{20}$$

as a matrix generalization of the result given by Edwards and Muthukumar [33] and Ohta and Kawasaki [42]. Equation (20) has not been proven yet, but it can be done very easily by separating out several chains of types σ and τ in Eq. (8), and integrating out the Φ's and ρ's providing, e.g.,

$$\begin{aligned}\mathcal{H}_1(\mathbf{R}^{\sigma}_1,\mathbf{R}^{\tau}_1)=&\int_0^{N^{\sigma}}ds\left[\frac{\partial\mathbf{R}^{\sigma}_1(s)}{\partial s}\right]^2+\int_0^{N^{\tau}}ds\left[\frac{\partial\mathbf{R}^{\tau}_1(s)}{\partial s}\right]^2+\int_0^{N^{\sigma}}\int_0^{N^{\sigma}}ds\,ds'U^{\text{eff}}_{\sigma\sigma}[\mathbf{R}^{\sigma}_1(s)-\mathbf{R}^{\sigma}_1(s')]\\&+\int_0^{N^{\tau}}\int_0^{N^{\tau}}ds\,ds'U^{\text{eff}}_{\tau\tau}[\mathbf{R}^{\tau}_1(s)-\mathbf{R}^{\tau}_1(s')]+2\int_0^{N^{\sigma}}\int_0^{N^{\tau}}ds\,ds'U^{\text{eff}}_{\sigma\tau}[\mathbf{R}^{\sigma}_1(s)-\mathbf{R}^{\tau}_1(s')]\ ,\end{aligned} \tag{21}$$

where $U_{\sigma\tau}$ are precisely the matrix elements of the matrix (20). Nevertheless these are some severe subtleties in deriving Eq. (20) by this method and the original derivation of Edwards, as will be shown in a forthcoming publication. So far the formulation is general for arbitrary multicomponent systems and the specification to diblock copolymers is simple. Equation (21) reads in this case

$$\begin{aligned}\mathcal{H}_1(\mathbf{R}_1)=&\int_0^{N}ds\left[\frac{\partial\mathbf{R}(s)}{\partial s}\right]^2\\&+\int_0^{fN}ds\int_0^{fN}ds'U^{\text{eff}}_{AA}[\mathbf{R}_A(s)-\mathbf{R}_A(s')]\\&+\int_{fN}^{N}ds\int_{fN}^{N}ds'U^{\text{eff}}_{BB}[\mathbf{R}_B(s)-\mathbf{R}_B(s')]\\&+2\int_0^{fN}ds\int_{fN}^{N}ds'U^{\text{eff}}_{AB}[\mathbf{R}_A(s)-\mathbf{R}_B(s')]\end{aligned} \tag{22}$$

and

$$\underline{S}^{0}(\mathbf{k})=\begin{bmatrix}S^{0}_{AA}&S^{0}_{AB}\\S^{0}_{BA}&S^{0}_{BB}\end{bmatrix}, \tag{23}$$

$$\begin{aligned}\underline{V}(\mathbf{k})&=\begin{bmatrix}V_{AA}&V_{AB}\\V_{BA}&V_{BB}\end{bmatrix}\\&\equiv\begin{bmatrix}V&V+\chi_F\\V+\chi_F&V\end{bmatrix}.\end{aligned} \tag{24}$$

The inversion defines the effective potential (20) between two arbitrary monomers in the melt, and also a tagged chain in the melt,

$$U^{\text{eff}}_{AA}(\mathbf{k})=\frac{[1-2\chi_F S^{0}_{BB}(\mathbf{k})]/\det\underline{S}^{0}}{S^{0}_{T}/\det\underline{S}^{0}-2\chi_F}\ , \tag{25}$$

$$U^{\text{eff}}_{BB}(\mathbf{k})=\frac{[1-2\chi_F S^{0}_{AA}(\mathbf{k})]/\det\underline{S}^{0}}{S^{0}_{T}/\det\underline{S}^{0}-2\chi_F}\ , \tag{26}$$

$$U^{\text{eff}}_{AB}(\mathbf{k})=\frac{[1+2\chi_F S^{0}_{AB}(\mathbf{k})]/\det\underline{S}^{0}}{S^{0}_{T}/\det\underline{S}^{0}-2\chi_F}\ , \tag{27}$$

which has been given in [36,43]. Note that these effective potentials have unphysical singularities at the microphase separation condition. This is a result of the mean-field approximation on the Gaussian level.

The "bare" structure factors in Eqs. (25)–(27) are given by (f is the volume fraction of species A)

$$S^{0}_{AA}(\mathbf{k})=(N_A+N_B)P_A(f,\mathbf{k})\ , \tag{28}$$

$$S^{0}_{BB}(\mathbf{k})=(N_A+N_B)P_B(1-f,\mathbf{k})\ , \tag{29}$$

$$S^{0}_{AB}(\mathbf{k})=S^{0}_{BA}(\mathbf{k})=(N_A+N_B)P_{AB}(f,\mathbf{k})\ , \tag{30}$$

where $P_A(f,\mathbf{k})$, $P_B(1-f,\mathbf{k})$, and $P_{AB}(f,\mathbf{k})$ are the intramolecular form factors for the two blocks A and B and the intramolecular interference form factor between the blocks. These form factors are conveniently represented by modified Debye functions, if we assume Gaussian unperturbated copolymer chains for the bare state

$$P_A(f,\mathbf{k})=\frac{2}{u^2}(e^{-fu}+fu-1)\ , \tag{31}$$

$$P_B(1-f,\mathbf{k})=\frac{2}{u^2}[e^{-(1-f)u}+(1-f)u-1]\ , \tag{32}$$

$$P_{AB}(f,\mathbf{k})=\tfrac{1}{2}[P_A(1,\mathbf{k})-P_A(f,\mathbf{k})-P_B(1-f,\mathbf{k})]\ . \tag{33}$$

In this notation we set $u=\mathbf{k}^2R_g^2$ with R_g the radius of gyration of the whole diblock copolymer. Figure 2(a) shows the effective potential of one block of a symmetric diblock copolymer (i.e., $f=\frac{1}{2}$) in $\mathbf{k}$ space, which is attractive, whereas the effective potential $U^{\text{eff}}_{AB}(\mathbf{k})$ is repulsive [Fig. 2(b)].

It can be shown easily that the potential $U^{\text{eff}}_{\sigma\tau}$ ($\sigma,\tau=A,B$) is not restricted to monomers on one chain. $U^{\text{eff}}_{\sigma\tau}$ is the effective potential of two arbitrary monomers of type σ,τ in the melt, i.e.,

$$U^{\text{eff}}_{AB}[\mathbf{R}^{A}_{\alpha}(s)-\mathbf{R}^{B}_{\beta}(s')]=\int\frac{d^3k}{(2\pi)^3}U^{\text{eff}}_{AB}(\mathbf{k})e^{i\mathbf{k}\cdot(\mathbf{R}^{A}_{\alpha}(s)-\mathbf{R}^{B}_{\beta}(s'))}\ . \tag{34}$$

The Fourier transform (FT) in Eq. (34) cannot be carried

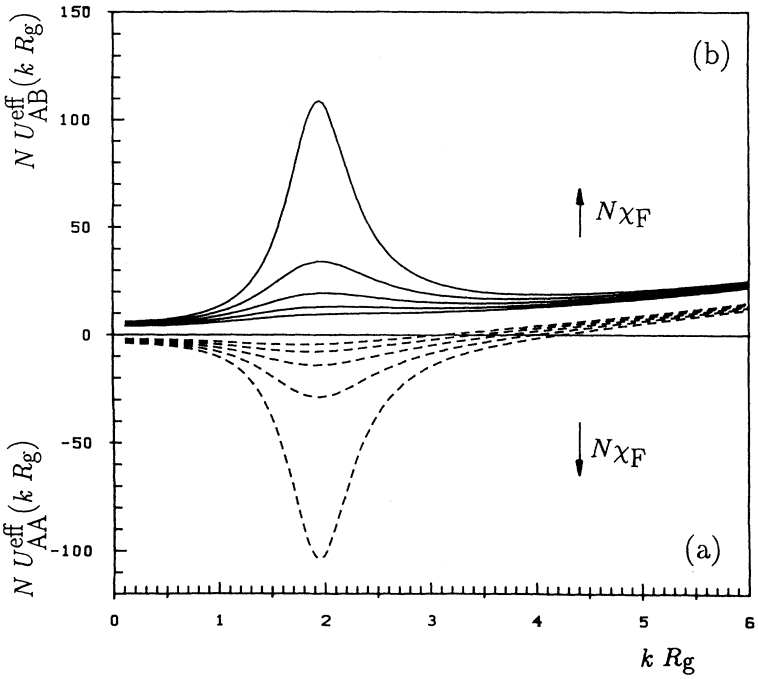

FIG. 2. (a) Effective potential between monomers of the same species. (b) Effective potential between different types of monomers. In both cases, $\chi_F N$ has the values 6, 7, 8, 9, and 10 in the direction of the arrow.

out analytically without making uncontrollable approximations. Numerical FT can be performed and shows oscillating behavior with a characteristic period roughly to the radius of gyration, which is the only relevant length scale in the one-phase region above $k_B T_c$. Our main discussion is restricted to the representation in k space.

A perturbation calculation of R_g has been outlined in Refs. [37,44], but it is not clear to which distance $(\chi_0 - \chi_F)$ its results are reliable, due to the unphysical singularity. Nevertheless it has been shown (and is physically obvious) that the individual blocks shrink near the microphase separation transition (MST) [43] as in polymer blends [44], since both U^{eff}_{AA} and U^{eff}_{BB} change sign near the MST. The $U^{\text{eff}}_{\text{AB}}$ potential is always positive. The two blocks separate from another, i.e., the whole chains stretch at the critical point. These arguments are strongly supported by this work and by simulations of Fried and Binder [18] as we will show below.

IV. RESULTS—DENSE MELT

In the athermal limit, i.e., $\varepsilon_{ij}/k_B T \to 0$, no interactions between the monomers apart from the excluded volume constraints are present. Starting from an athermal configuration, we cool the system by lowering the temperature to the simulation temperature. The ensembles of configurations at the different temperatures are created independently. As an indication that our system which consists of n_{polymers} chains is relaxed, we consider the correlation of the end-to-end vector of the total chain

$$C_{\text{end}}(n_{\text{MCS}}) = \frac{1}{n_{\text{polymers}}} \sum_{i=1}^{n_{\text{polymers}}} \frac{\mathbf{R}^i_{\text{end}}(n_{\text{MCS}}=0)\cdot\mathbf{R}^i_{\text{end}}(n_{\text{MCS}})}{|\mathbf{R}^i_{\text{end}}(n_{\text{MCS}}=0)||\mathbf{R}^i_{\text{end}}(n_{\text{MCS}})|} \tag{35}$$

and take twice the n_{MCS} Monte Carlo steps (MCS) needed for a decay to zero as thermalization steps. The number of Monte Carlo steps is strongly dependent on the temperature $k_B T/\varepsilon$ and on the chain length N. For example, 9000 (360 000) Monte Carlo steps per chain (MCS/chain) are needed for $N=20$ and $k_B T/\varepsilon > k_B T_c/\varepsilon$ ($k_B T/\varepsilon < k_B T_c/\varepsilon$), if we define a Monte Carlo step as an attempt to move a whole chain element. (As we only concentrate on static properties, this somehow arbitrary definition does not affect our results, and is only chosen for a proper counting of the simulation steps.) During those steps, all chains have turned on average about 180° in orientation and we expect the chains to have found their equilibrium configuration at this given temperature $k_B T/\varepsilon$. After this thermalization, sampling starts for the thermodynamic averages every 1000 MCS/chain over a Monte Carlo step span of between 500 000–1 500 000 MCS/chain. The computer runs were carried out on DEC stations 5000/125 and 5000/200.

To compare our results to those of the literature we notice the connection between the Flory χ_F parameter and the temperature $k_B T/\varepsilon$ in our simulation. It is given by

$$\chi_F = \frac{(q-2)\varepsilon}{k_B T} . \tag{36}$$

In our case $\varepsilon = \varepsilon_{AB}$, $q=12$, and $k_B = 1$. Leibler's mean-field prediction [20] for the location of the critical point is $(\chi_F N)_c = 10.495$, and the result of Fredrickson and Helfand, which includes fluctuations of the order-parameter correlations, postulates $(\chi_F N)_c = 10.495 + 41 N^{-1/3}$ [10]. We therefore expect $k_B T/\varepsilon N$ to be a good scaling variable for large chain lengths N.

In the preceding section we derived the intramolecular potentials U^{eff}_{AA}, or U^{eff}_{BB} [Fig. 2(a)], and U^{eff}_{AB} [Fig. 2(b)]. The effective force

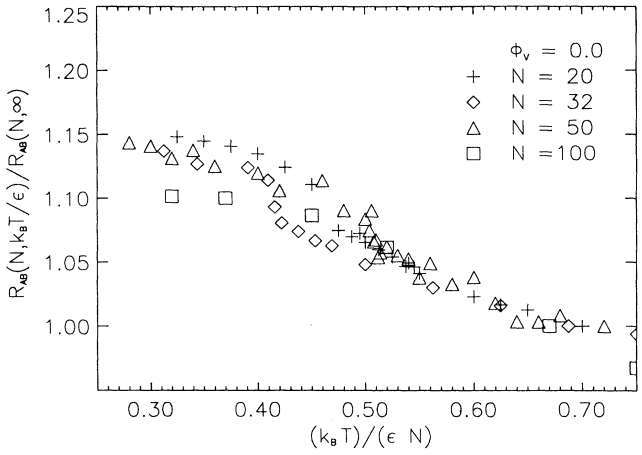

FIG. 3. Temperature dependence of the distance between the centers of mass of the two blocks. Chain lengths are $N=20$, 32, 50, and 100.

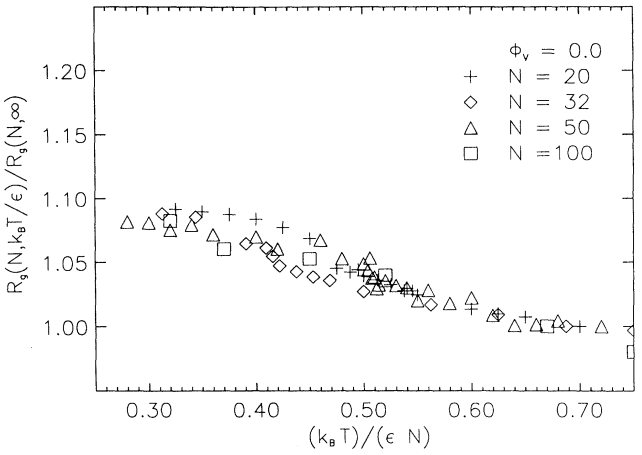

FIG. 5. Temperature dependence of the radius of gyration. Chain lengths are $N=20$, 32, 50, and 100.

$$\mathbf{F}_{\sigma\tau}=-\nabla U^{\text{eff}}_{\sigma\tau}(\mathbf{r})=\sum_{\mathbf{k}} i\mathbf{k}U^{\text{eff}}_{\sigma\tau}(\mathbf{k}) \tag{37}$$

acting between the monomers σ,τ of different blocks of one chain in the medium of all others is repulsive, while the force acting between the same species of monomers in one block is attractive. The simulations confirm these mean-field results as the distance between the centers of mass of the two blocks,

$$R_{AB}=[\langle(\mathbf{R}^{A}_{\text{c.m.}}-\mathbf{R}^{B}_{\text{c.m.}})^2\rangle]^{1/2}\,, \tag{38}$$

increases according to the repulsive effective potential (Fig. 3). Here, $\mathbf{R}^{\alpha}_{\text{c.m.}}$ is the center of mass of a single block $\alpha=A,B$, while the radius of gyration of one block R_g^{α} remains almost constant (Fig. 4). Note that the scale for R_g^{A} is different from Fig. 3.

As already mentioned in the preceding section, one would expect [43] the two separate blocks to behave like A and B homopolymers in a blend due to the attractive effective potential. In this case they are supposed to shrink. That they do not shrink can be understood by the relatively short chain lengths and therefore by the rather small wavelength of the developing structure. The rather long chains with $N=100$ show a slight decrease of the radius of gyration of one block when the temperature is decreased. The radius of gyration of the total chains ($\mathbf{r}_j^i$ being the space coordinate of the monomers)

$$R_g=\left[\frac{1}{n_{\text{polymers}}N}\sum_{i=1}^{n_{\text{polymers}}}\sum_{j=1}^{N}(\mathbf{r}_j^i-\mathbf{R}^i_{\text{c.m.}})^2\right]^{1/2} \tag{39}$$

shows an increase by 10% (Fig. 5), and the end-to-end distance of the chains

$$R_{\text{end}}=\left[\frac{1}{n_{\text{polymers}}}\sum_{i=1}^{n_{\text{polymers}}}(\mathbf{r}_N^i-\mathbf{r}_1^i)^2\right]^{1/2} \tag{40}$$

increases remarkably as well (Fig. 6). Similar results have

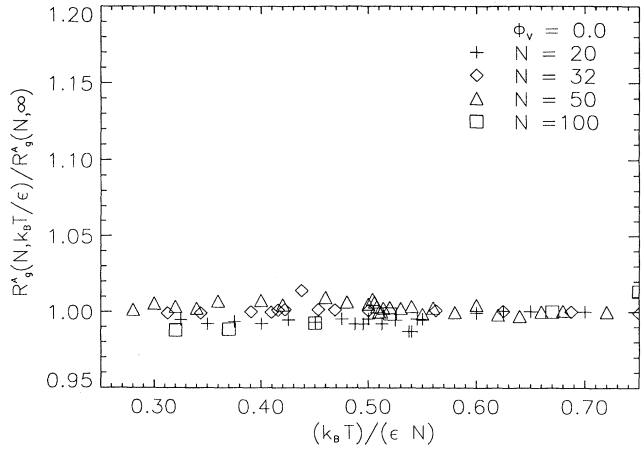

FIG. 4. Temperature dependence of the radius of gyration of one block. Chain lengths are $N=20$, 32, 50, and 100.

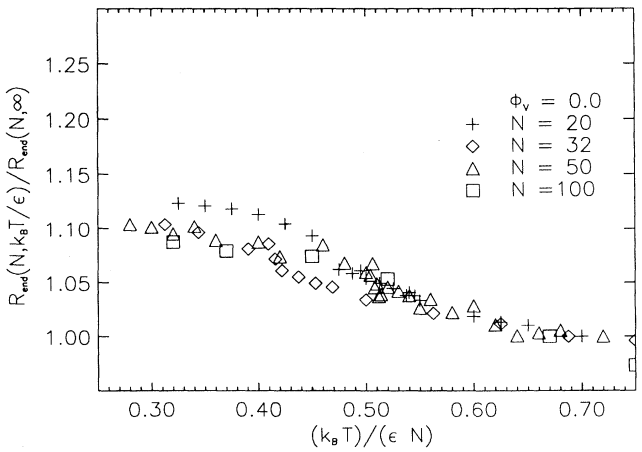

FIG. 6. Temperature dependence of the end-to-end vector. Chain lengths are $N=20$, 32, 50, and 100.

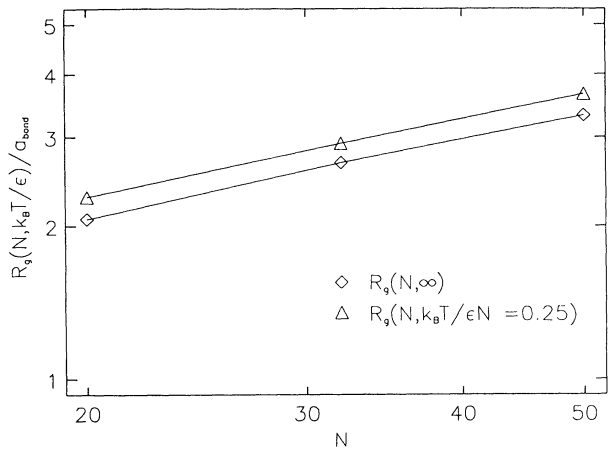

FIG. 7. Radius of gyration vs chain length. Both in the athermal limit and in the finite temperature range the chains are found to be Gaussian, as the slope of the curves have been found to be approximately $\nu=0.51$.

already been found in experiments [45,4].

In the athermal limit the diblock chains are expected to behave in a Gaussian manner:

$$R_g \sim N^{\nu} , \tag{41}$$

where $\nu=\frac{1}{2}$ is predicted. An evaluation of $\ln R_g$ vs $\ln N$ (Fig. 7) yields an exponent $\nu=0.510$, which is very close to the random walk. Therefore in uniform dense melts ($\varepsilon_{AB}=\varepsilon=0\equiv\chi_F=0$) excluded volume effects are screened. But also in the finite temperature limit ($\chi_F\neq 0$) and even at a temperature just below the critical value the exponent $\nu=0.511$ indicates Gaussian behavior of the chains (also Fig. 7). This shows that the exponent ν is not altered for $\chi_0-\chi_F>0$. In the strong segregation limit we could expect $\nu=\frac{2}{3}$ [42], but our simulations do not confirm this. Again the short chains could be responsible for this since the $\frac{2}{3}$ result holds only in the scaling limit $N\rightarrow\infty$.

There are several possibilities to determine whether or not the two species are demixed at a given temperature. The simplest way is to look at the monomer distribution in a small subvolume of the system. In the disordered phase the probability distribution of finding a monomer of species A, $p(\phi_A)$, in a box of volume l^3 is Gaussian. At the microphase separation transition, two phases rich in either species A or B appear and the probability distribution become bimodal (Fig. 8). One has to choose the subvolume l^3 carefully, as it should be adapted to the chain length and by that reason to the periodicity of the arising structure. In Fig. 8 we see the temperature evolution of the probability distribution for the concentration of A monomers $p(\phi_A)$ of chains with $N=32$ in a subvolume $(l=6)^3$. The two maxima at temperatures below the microphase separation correspond to the equilibrium concentrations of the two phases at this temperature. The strong interface effects are due to the connectivity of the two blocks. This hinders a finite-size-like analysis for the location of k_BT_c/ε as in [46].

Another possibility is to mark the different types of monomers by different colors and to view them. Those snapshots are presented in Fig. 9, where we show four stages of a diblock copolymer melt (remembering periodic boundary conditions we used in this representation). Figure 9(a) reflects the melt at a temperature far above from the transition point. The two species are distributed homogeneously, which is also monitored in the Gaussian

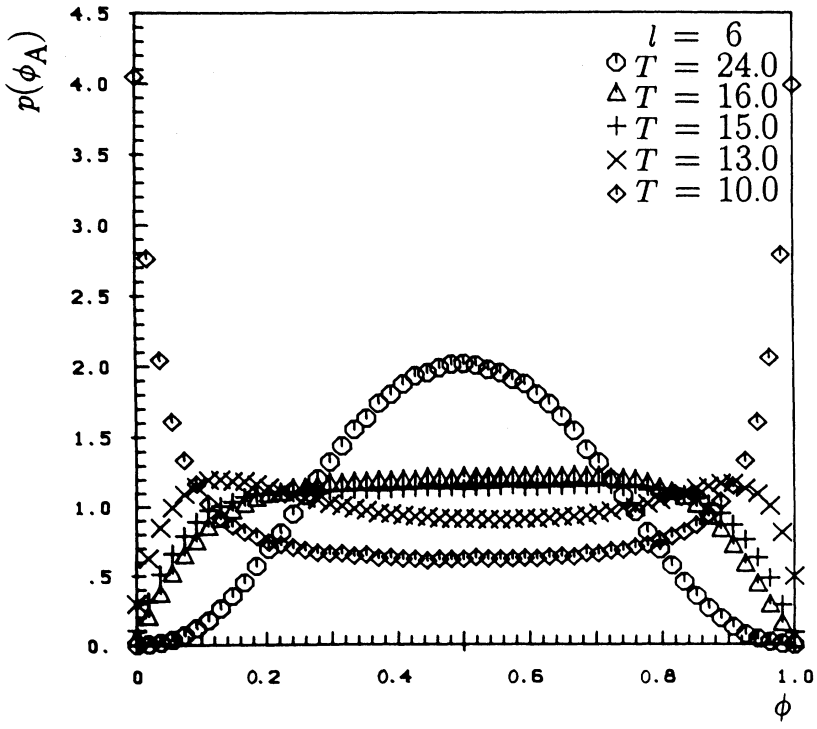

FIG. 8. The probability distribution of the concentration of species A in a subvolume l^3 changes the shape with decreasing temperature ($k_B=\varepsilon=1$). We present an example for a melt of $N=32$ and box size $(l=6)^3$. Above the critical temperature the distribution is Gaussian. It becomes bimodal below k_BT_c/ε.

distributed A monomer concentration of Fig. 8. A few temperature steps above $k_B T_c/\varepsilon$ we already observe [Fig. 9(b)] concentration fluctuations, and when we reach $k_B T_c/\varepsilon$ [Fig. 9(c)] first indications of an ordered structure can be seen. Below the microphase separation transition for the diblock copolymer melt a clear lamellar structure is found [Fig. 9(d)].

As a consequence of the microphase separation and the stretching of the chains, an orientational ordering of the chains occurred. We looked at the correlation of the vector connecting the centers of mass of the two blocks with an arbitrarily chosen direction, for example, the (1,0,0) direction. In the disordered state the second harmonical Legendre polynomial (i.e., the orientational parameter) f,

$$f=\tfrac{1}{2}(3\langle\cos^2\vartheta\rangle-1)\ , \tag{42}$$

is fluctuating around zero, while at a certain temperature this orientational parameter reaches a finite value (Fig.

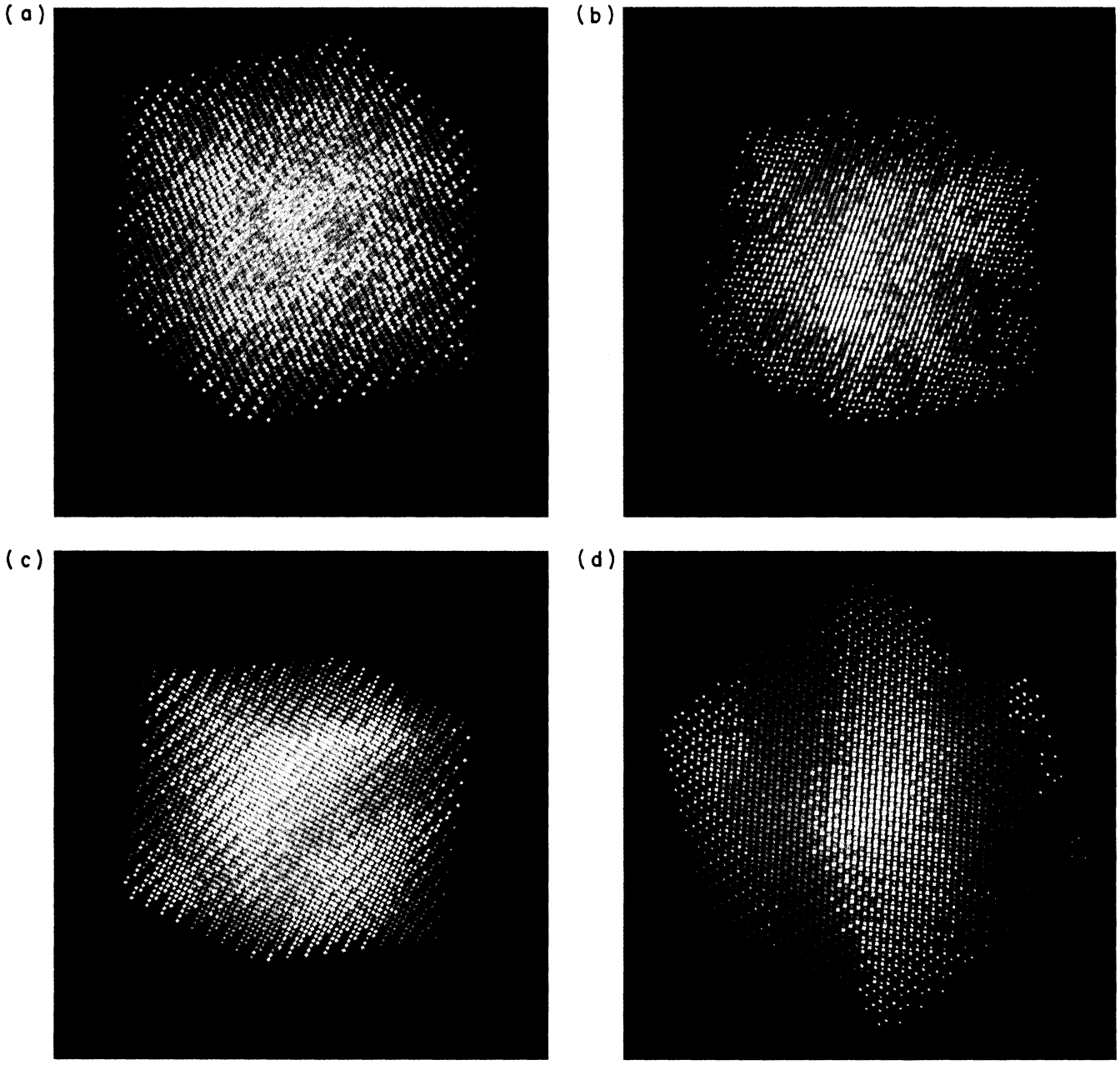

FIG. 9. Snapshots of an $N=20$ diblock copolymer melt at different temperatures. The green and white symbols refer to the different types of monomers, whereas bonds have been omitted for a better overview. The value of $k_B T_c/\varepsilon$ is taken from the specific heat (Fig. 11) for $N=20$. (a) At $k_B T/\varepsilon=20 \gg k_B T_c/\varepsilon$ the melt is homogeneously mixed. (b) Above $k_B T_c/\varepsilon$ ($k_B T/\varepsilon=14$) compositional fluctuations can already be observed. (c) At the critical point of the melt, a lamellar structure arises ($k_B T/\varepsilon \sim 9.0$). (d) A few temperature steps below $k_B T_c/\varepsilon$ ($k_B T/\varepsilon=8$) a clear lamellar structure has been developed.

10). This effect can be understood by the following intuitive picture: as the two types of monomers separate into two homogeneous phases rich in either species A or B, and as the chains become stretched at the microphase separation transition, the chains have to order with respect to their mean axis, as they are close packed. Due to this ordering, a finite orientational parameter can be observed. This has novel theoretical impact special for the nature of the MST in block copolymers. A detailed study has been performed and will be published separately [47]. This ordering temperature depends slightly on the chain length, as for increasing chain length it is shifted towards lower temperatures. It is found to be in the range $k_B T_c/\varepsilon N \approx 0.45-0.5$. During the simulation, the entire lamellar structure reorientates several times in the simulation box. For the sake of simplicity we considered the orientational parameter only in respect to an arbitrarily chosen direction and not to the mean direction of the chains. Therefore the shape of the curve in the critical region must not be interpreted as a universal shape.

The specific heat C_V is expected to show a peak at the critical temperature for phase transitions of either first or second order in finite systems. According to usual Monte Carlo simulations the specific heat is calculated via the fluctuation-dissipation theorem

$$C_V = \frac{1}{k_B T^2}(\langle E^2\rangle - \langle E\rangle^2) . \tag{43}$$

In analogy to spin systems we plot the value of the specific heat per chain (Fig. 11). Analyzing the specific heat yields a value for $k_B T_c/\varepsilon N$ which is dependent on the chain length. The transition region can be identified to be $k_B T_c/\varepsilon N \approx 0.45-0.5$. Comparing it to the ordering temperature for the orientational parameter, we find that they seem to coincide. In view of Ref. [47] this has to be reexamined. Our simulation results expressed in terms of the Flory parameter locate the transition regime at $(\chi_F N)_c \approx 19.8-22.2$, whereas the predictions of Fredrickson and Helfand for the given lengths yield $(\chi_F N)_c = 21.62-25.59$. The critical temperature, which is inversely proportional to $(\chi_F N)_c$, is in rather good agreement with the prediction of Fredrickson and Helfand (Fig. 12); the values for $k_B T_c/\varepsilon$ lie only about 5.6% to 13.3% above their values. This is not necessarily expected, as the Hartree approximation used by Fredrickson and Helfand should be correct for $N \gtrsim 10^9$. Even though these authors argue that for block copolymers their estimation should apply for chain lengths of $N \sim 10^4$, our case is below that limit, and it is rather surprising that the theory explains our results not only qualitatively well, but also quantitatively.

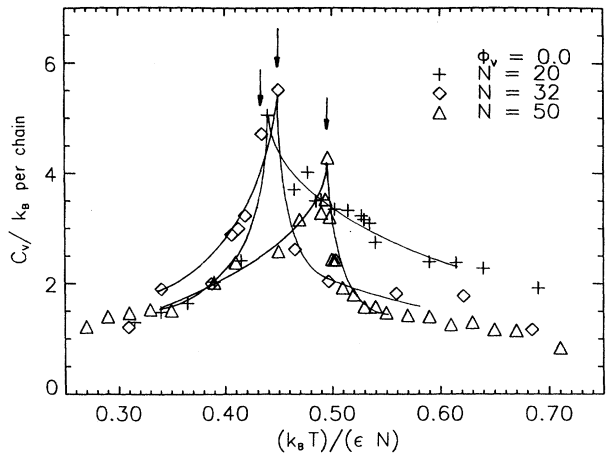

FIG. 11. The position of the maximum of the specific heat. The arrows denote the critical temperature $k_B T_c(N)/\varepsilon$ for the different chain lengths. It is slightly shifted towards lower values of $k_B T/\varepsilon N$ for increasing chain length ($N=20$, 32, and 50). The lines are only guides to the eye.

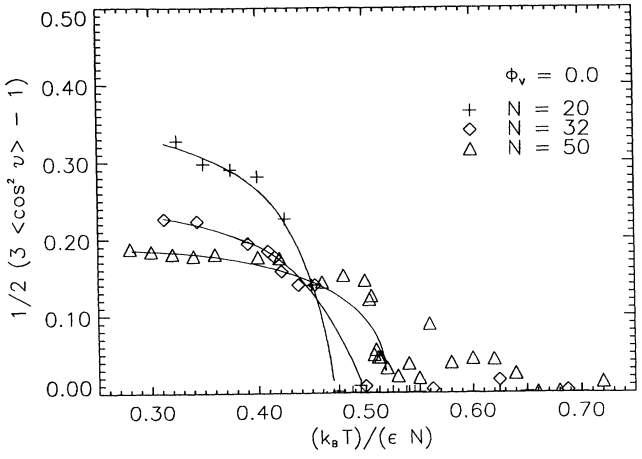

FIG. 10. The orientational parameter f reaches a finite value at the ordering temperature, when the system is cooled down. The transition point is slightly shifted towards lower values of $k_B T/\varepsilon N$ for increasing chain length ($N=20$, 32, and 50). It seems to coincide with the critical temperature. The lines are only guides to the eye.

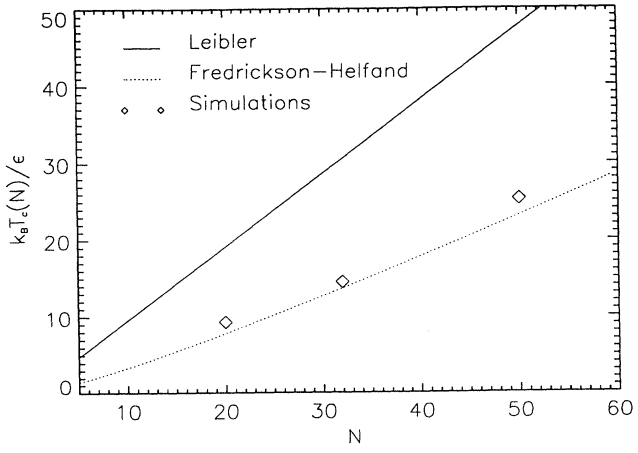

FIG. 12. Critical temperature in dependence of the chain length. The solid line represents Leibler's predictions, the dashed line is the result of Fredrickson and Helfand, and the symbols are our simulations results, taken from the specific heat (Fig. 11).

V. EFFECTS OF VACANCIES (MEAN-FIELD PREDICTIONS)

Two basically different types of simulations have been made: first at density $\phi=1$, i.e., no presence of vacancies, and second at $\phi<1$, i.e., presence of vacancies. The RPA is appropriate to deal with the situation [44,48,49]. Here we recall early work of Benoit and Benmouna [48] which was not intended to describe the effect of vacancies but for solvent molecules, which play essentially the same role. The basic difference is that the vacancies can be treated as a third component in a binary system (A and B molecules). The Edwards Hamiltonian in matrix formulation is then given by [50]

$$\mathcal{H}=\boldsymbol{\rho}[(\underline{S}^0)^{-1}(\mathbf{k})+\underline{V}]\boldsymbol{\rho} \ , \tag{44}$$

where

$$\boldsymbol{\rho}=(\rho_{\mathbf{k}}^A,\rho_{\mathbf{k}}^B,\rho^V) \tag{45}$$

and

$$\underline{S}^0(\mathbf{k})=\begin{bmatrix} S_{AA}^0 & S_{AB}^0 & 0 \\ S_{BA}^0 & S_{BB}^0 & 0 \\ 0 & 0 & S_V^0 \end{bmatrix} , \tag{46}$$

$$\underline{V}(\mathbf{k})=\begin{bmatrix} V_{AA} & V_{AB} & V_{AV} \\ V_{BA} & V_{BB} & V_{BV} \\ V_{VA} & V_{VB} & V_{VV} \end{bmatrix} , \tag{47}$$

where S_V^0 is the structure factor of the vacancies. Since they are distributed at random and they are assumed not to have any structure it can be written simply as

$$S_V^0=\phi_V \ , \tag{48}$$

where ϕ_V is the volume fraction of the vacancies. The $V_{\sigma\tau}$ $(\sigma,\tau=A,B,V)$ are the potentials between the different components. The effective three-component system is now characterized by

$$\phi_A(\mathbf{r})+\phi_B(\mathbf{r})+\phi_V(\mathbf{r})=1 \tag{49}$$

or

$$\rho_{\mathbf{k}}^V=-(\rho_{\mathbf{k}}^A+\rho_{\mathbf{k}}^B) \ , \tag{50}$$

where $\phi_\sigma(\mathbf{r})=\phi_\sigma+\rho^\sigma(\mathbf{r})$. The condition (50) leads to an effective two-component Hamiltonian [50] with effective interactions, i.e.,

$$\mathcal{H}_{\text{eff}}^{AB}=\boldsymbol{\rho}\underline{S}^{-1}\boldsymbol{\rho} \ , \tag{51}$$

with $\boldsymbol{\rho}=(\rho_{\mathbf{k}}^A,\rho_{\mathbf{k}}^B)$ and an inverse correlation matrix

$$\underline{S}^{-1}(\mathbf{k})=\underline{S}_{\text{eff}}^{-1}+\underline{U}_{\text{ex vol}} \ , \tag{52}$$

with

$$\underline{S}_{\text{eff}}^{-1}(\mathbf{k})=\frac{1}{\det\underline{S}^0}\begin{bmatrix} S_{BB}^0 & -S_{AB}^0 \\ -S_{AB}^0 & S_{AA}^0 \end{bmatrix} \tag{53}$$

and the excluded volume matrix

$$\underline{U}_{\text{ex vol}}=\begin{bmatrix} \frac{1}{\phi_V}+(V_{AA}+V_{SS}-2V_{AS}) & \frac{1}{\phi_V}+V_{SS}+V_{AB}-V_{AS}-V_{BS} \\ \frac{1}{\phi_V}+V_{SS}+V_{AB}-V_{AS}-V_{BS} & \frac{1}{\phi_V}+(V_{BB}+V_{SS}-2V_{BS}) \end{bmatrix} , \tag{54}$$

which is the usual excluded volume matrix if V is a solvent S [50]. For our purpose and without loss of generality we may set

$$V_{\sigma\tau}=0 \quad \forall\sigma,\tau \text{ except } V_{AB}=V+\chi_F \ , \tag{55}$$

i.e., the vacancies do not interact with any other component. (For a more general treatment see Kehr, Binder, and Reulein [51].)

Then we have

$$\underline{U}_{\text{ex vol}}=\begin{bmatrix} \frac{1}{\phi_V} & \frac{1}{\phi_V}+\chi_F \\ \frac{1}{\phi_V}+\chi_F & \frac{1}{\phi_V} \end{bmatrix} . \tag{56}$$

The stability criterion is given by

$$\det\underline{S}^{-1}=0 \ . \tag{57}$$

This yields the mean-field shift of the spinodal of block copolymers on a simple basis by the evaluation of the determinant. We keep the terms to order χ_F^2 in order to include the case that ϕ_V is not close to 0, but eventually $\phi_V \lesssim \frac{1}{2}$:

$$\det\begin{bmatrix} \frac{S_{BB}^0}{\det\underline{S}^0}+1 & -\frac{S_{AB}^0}{\det\underline{S}^0}+\frac{1}{\phi_V}+\chi_F \\ -\frac{S_{AB}^0}{\det\underline{S}^0}+\frac{1}{\phi_V}+\chi_F & \frac{S_{AA}^0}{\det\underline{S}^0}+\frac{1}{\phi_V} \end{bmatrix}=0 \ . \tag{58}$$

Equation (58) produces the quadratic equation for the stability condition

$$\left[\frac{S_{AA}^0}{\det\underline{S}^0}+\frac{1}{\phi_V}\right]\left[\frac{S_{BB}^0}{\det\underline{S}^0}+\frac{1}{\phi_V}\right]-\left[-\frac{S_{AB}^0}{\det\underline{S}^0}+\frac{1}{\phi_V}+\chi_F\right]^2=0 \ . \tag{59}$$

Therefore the critical χ_F value is given by

$$\chi_c(\mathbf{k})=\left\{\left[\frac{S^0_{AA}}{\det\underline{S}^0}+\frac{1}{\phi_V}\right]\left[\frac{S^0_{BB}}{\det\underline{S}^0}+\frac{1}{\phi_V}\right]\right\}^{1/2}+\frac{S^0_{AB}}{\det\underline{S}^0}-\frac{1}{\phi_V}\ . \tag{60}$$

In the limit of $\phi_V\to 0$ the square root can be expanded and simple algebra leads to

$$\chi_c(\mathbf{k})\cong\frac{1}{2}\left\{\frac{S^0_T(\mathbf{k})}{\det\underline{S}^0(\mathbf{k})}+\phi_V\frac{S_{AA}S^0_{BB}}{(\det\underline{S}^0)^2}+O(\phi_V^2)\right\}\ . \tag{61}$$

At $\phi_V=0$, $\chi_c(\mathbf{k})$ obeys the classical criterion of Leibler [20].

For a binary blend ($S^0_{AB}=0$) the critical value $\chi_c(\mathbf{k}=0)$ from (60) reads

$$\chi_c=\left\{\left[\frac{1}{N_A\phi_A}+\frac{1}{\phi_V}\right]\left[\frac{1}{N_B\phi_B}+\frac{1}{\phi_V}\right]\right\}^{1/2}-\frac{1}{\phi_V}\ , \tag{62}$$

which is to order of ϕ_V equivalent to

$$\frac{\phi_V}{\phi_A\phi_B}\frac{1}{N_AN_B}+2(\chi_0-\chi_F)=0\ , \tag{63}$$

where $2\chi_0=1/N_A\phi_A+1/N_B\phi_B$. Thus the well-known result, that vacancies produce a slight compatability enhancement, has been reproduced. Again for $\phi_V\to 0$ the classical condition for the phase separation on the macroscopic level is recovered. The structure factors can be given in the usual sense, for example, we find for $S_{AA}(\mathbf{k})$

$$S_{AA}(\mathbf{k})=\frac{1}{\det(\underline{S}^{-1}_{\text{eff}}+\underline{U}_{\text{ex vol}})}\left[\frac{S^0_{BB}(\mathbf{k})}{\det\underline{S}^0}+\frac{1}{\phi_V}\right]\ , \tag{64}$$

which can be rewritten as

$$S_{AA}(\mathbf{k})=\frac{1+\phi_V\dfrac{S^0_{AA}(\mathbf{k})}{\det\underline{S}^0}}{\left[\dfrac{S^0_{AA}}{\det\underline{S}^0}+\dfrac{1}{\phi_V}\right]\left[\dfrac{S^0_{BB}}{\det\underline{S}^0}+\dfrac{1}{\phi_V}\right]-\left[-\dfrac{S^0_{AB}}{\det\underline{S}^0}+\dfrac{1}{\phi_V}+\chi_F\right]^2}\ . \tag{65}$$

Again for $\phi_V\to 0$ Leibler's result is recovered.

The next step is to show the effect of vacancies on the effective potentials. This can be done along the same lines as outlined in Sec. III. The effective potentials are given by

$$\underline{U}_{\text{eff}}=(\underline{S}_{\text{eff}}+\underline{U}^{-1}_{\text{ex vol}})^{-1}\ . \tag{66}$$

Carrying out the matrix inversion we find for the $U^{\text{eff}}_{\sigma\tau}$ potentials

$$U^{\text{eff}}_{AA}(\mathbf{k})=\frac{1-(2\chi_F+\phi_V\chi_F^2)S^0_{BB}}{\det\underline{S}^0\left[\dfrac{S^0_T}{\det\underline{S}^0}-(2\chi_F+\phi_V\chi_F^2)\right]+2\phi_V\chi_FS^0_{AB}+\phi_V} \tag{67}$$

and

$$U^{\text{eff}}_{AB}(\mathbf{k})=\frac{(2\chi_F+\phi_V\chi_F^2)S^0_{AB}+\phi_V\chi_F+1}{\det\underline{S}^0\left[\dfrac{S^0_T}{\det\underline{S}^0}-(2\chi_F+\phi_V\chi_F^2)\right]+2\phi_V\chi_FS^0_{AB}+\phi_V} \tag{68}$$

which reduce to all limits discussed so far, i.e., blends $S^0_{AB}=0$, and incompressibility $\phi_V\to 0$.

VI. RESULTS—EFFECTS OF VACANCIES

As most of the algorithms available for the simulation of polymer melts need a certain amount of vacancies ϕ_V to generate new polymer configurations [17–19,22–24], we analyzed the influence of vacancies on static thermodynamic properties of the copolymer melt. The vacancies are introduced as a good solvent, which means we have no interaction between the polymer and the vacancies and among the vacancies themselves, $\varepsilon_{AV}=\varepsilon_{BV}=\varepsilon_{VV}=0$. The vacancies will not separate from the polymers when the system is cooled.

A strong effect is that the chains become more extended in the presence of vacancies, more so the higher the vacancy concentration, both in the athermal limit and at finite temperatures. In Fig. 13 the temperature dependence of the radius of gyration R_g of a melt of copolymer chains with length $N=20$ is shown for vacancy concentrations $\phi_V=0.2,0.4$ compared to the results of the dense melt $\phi_V=0.0$. But if we plot the radius of gyration $R_g(k_BT/\varepsilon,N)$ of the given systems at temperature, k_BT/ε relative to the value in the athermal limit $R_g(\infty,N)$, no tendency can be detected that the chains

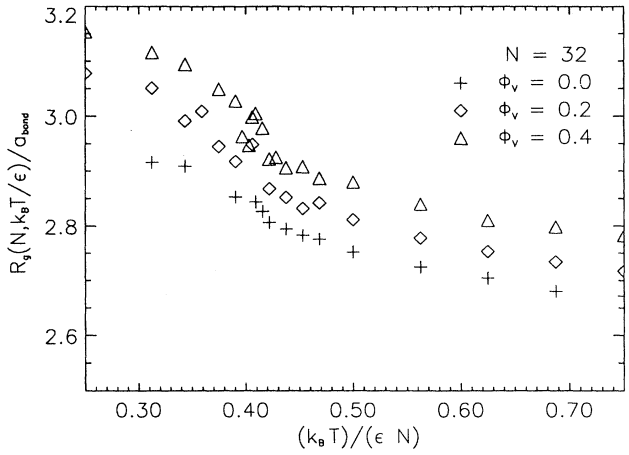

FIG. 13. Radius of gyration for $N=20$ and different vacancy concentrations $\phi_V=0.0,0.2,0.4$. In the presence of vacancies the chains are swollen.

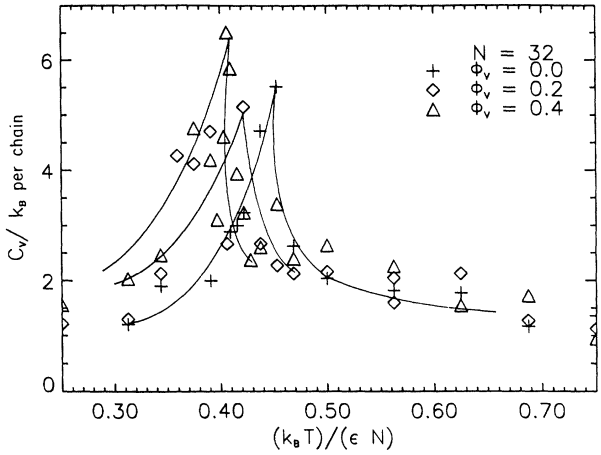

FIG. 15. The specific heat for $N=20$ and different vacancy concentrations $\phi_V=0.0,0.2,0.4$. The position of the maximum is shifted towards lower temperatures with increasing vacancy concentration. The vacancies reduce the incompatibility between the two species of monomers. The lines are only guides to the eye.

are stretched significantly more in the presence of vacancies. The curves seem to fall onto one master curve for all vacancy concentrations (Fig. 14). We conclude that the chains are swollen by the vacancies and that this effect is equal for the athermal limit and for finite temperatures. It can be observed for all radii presented in Sec. IV.

While considering the specific heat (Fig. 15) we find that the maximum of C_V is shifted towards lower temperatures for the systems with vacancies. The critical temperature for the system with 20% vacancies is lowered by 3.4–6.9 % compared to the dense system, while the system with higher vacancy concentration $\phi_V=0.4$ shows a transition temperature about 6.8–11.9 % below the values for the simulated dense melts. Hence, the higher the vacancy concentration is, the lower the critical temperature for a given chain length. This observation confirms the predictions of Eq. (59), that the vacancies produce a slight compatibility enhancement. At constant vacancy concentration the relative shift of the critical temperature for the different chain lengths is bigger for long chains ($N=50$) than for short chains ($N=20$).

Though species A separates from species B at the critical temperature given by the specific heat C_V and the chains stretch, the orientational temperatures from Fig. 16 seem to be lower than the critical points from C_V for all chain lengths observed (Fig. 16). This phenomenon is not easy to understand, as the vacancies are incorporated in the chains and do not leave more space for the stretched chains to lie in a disordered configuration for

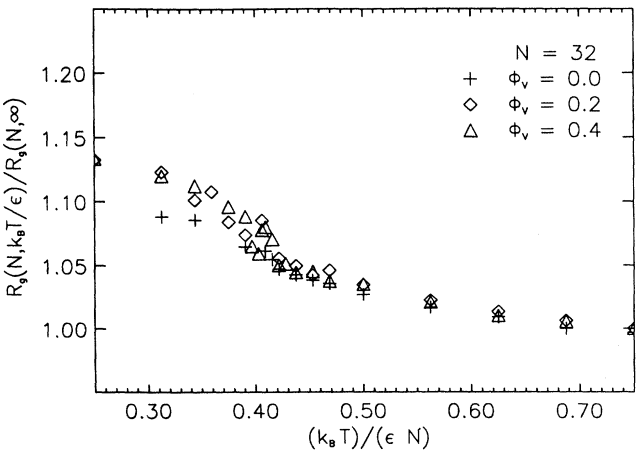

FIG. 14. Radius of gyration for $N=20$ and different vacancy concentrations $\phi_V=0.0,0.2,0.4$, normalized to the value at infinite temperature. The vacancies seem not to amplify the temperature-dependent stretching effect. Within the range of scattering the data seem to coincide on a master curve.

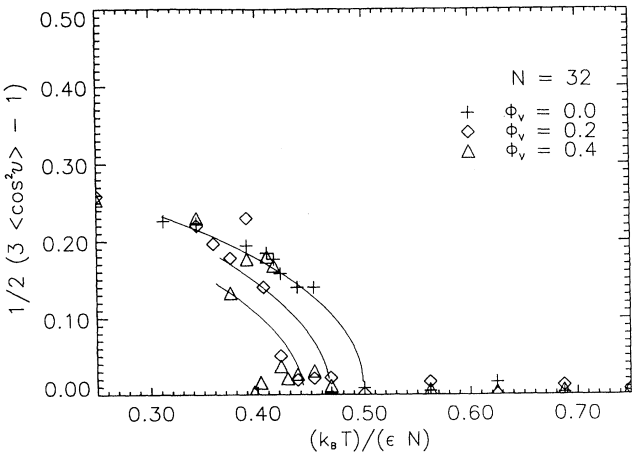

FIG. 16. The orientational parameter f for $N=20$ and different vacancy concentrations $\phi_V=0.0,0.2,0.4$. The ordering temperatures are shifted slightly more towards lower temperatures with increasing vacancy concentration than the position of the maximum of the specific heat. The lines are only guides to the eye.

lower temperatures. We plan to present an extented theoretical paper on this effect which includes other correlations than the density-density correlations. It can be shown explicitly that the orientational effects have a different critical temperature as given by the collective properties and the specific heat. It will also be shown that this is a typical copolymer effect and not present in blends for instance. It has also much impact on the dynamics of these systems. As already mentioned in Sec. IV the shape of the orientational parameter curve must not be understood as a universal law, as the correlation of the vector connecting the centers of mass of the A and the B block is taken only in respect to an arbitrarily chosen direction, i.e., the (1,0,0) direction, and not to a mean direction of the copolymer axes.

VII. SUMMARY

The thermodynamic behavior of diblock copolymers near the microphase separation transition has been studied in this paper. Using a random-phase approximation we could derive effective potentials $U_{\sigma\tau}^{\text{eff}}$ that describe the effective interactions between two arbitrary monomers of the different species σ,τ in the effective medium of the dense melt. With the use of repulsive U_{AB}^{eff} potential we can explain the stretching effect of the entire chains that has been observed in our simulation and also in experiments, from a perturbative view. Nevertheless the validity of the perturbation expansion is not quite clear, since the absolute values of the effective potential is not small, due to the increase near the transition. Therefore other methods, i.e., variational methods as the uniform expansion method used by Edwards, should be employed. Such variational methods are also able to change the exponents (as demonstrated by Edwards for dilute solutions). This could be sensible, since in the strong segregation limit the exponent ν is suggested to change from $\frac{1}{2}$ to $\frac{2}{3}$. The effective potential between monomers of the same species is attractive and therefore the blocks of our diblock copolymers are expected to shrink. This fact has been found in the simulation of long chains. The effective potentials show a nonphysical singularity at the microphase separation condition. This value for the singularity is located at the critical point, which is exactly the same found by Leibler in [20].

Once more it should be stressed that to our knowledge for the first time it was possible to simulate dense monodisperse diblock copolymer melts. We applied the cooperative motion algorithm that will be described explicitly in another publication [30]. The critical points of the simulated blockcopolymer melts have been found to be in rather good agreement with the fluctuation corrected predictions from Fredrickson and Helfand [10] in spite of principal difficulties for the applicability of the Brazovskii approximation arise in that limit of the chain length. The same difficulty appears of course in the Hartree approximation in classical solid-state physics. Below those critical temperatures the melts show a clear lamellar structure, as for symmetric diblock copolymers. Very close to the critical point we observed an ordering phenomenon in our simulation. The chains tend to order along a direction normal to the surface of the lamella. The theoretical description of this effect will be subject to a following publication [47].

As conventional Monte Carlo algorithms for the simulation of polymer melts need a certain amount of vacancies, we studied their influence on the critical behavior theoretically and by simulations. We have shown that the vacancies lower the critical temperature and thus weaken the incompatibility in the melt.

ACKNOWLEDGMENTS

We gratefully acknowledge Professor E. W. Fischer and Professor K. Binder for their interest in this work. For the stimulating discussions we also thank Professor M. Benmouna, Dr. M. G. Brereton, Dr. T. Pakula, and Dr. J. Reiter.

APPENDIX A: MEAN-FIELD TREATMENT OF VACANCIES: GENERAL PROPERTIES

In the main text we have shown that the scattering matrix and the effective potential matrix are given by

$$\underline{S}(\mathbf{k})=[\underline{S}^{0-1}(\mathbf{k})+\underline{V}]^{-1}\,, \tag{A1}$$

$$\underline{U}(\mathbf{k})=[\underline{S}^{0}(\mathbf{k})+\underline{V}^{-1}]^{-1}\,, \tag{A2}$$

where $\underline{V}$ is the excluded volume matrix

$$\underline{V}(\mathbf{k})=\begin{bmatrix} \frac{1}{\phi_V} & \frac{1}{\phi_V}+\chi_F \\ \frac{1}{\phi_V}+\chi_F & \frac{1}{\phi_V} \end{bmatrix}. \tag{A3}$$

The stability condition is

$$\det\underline{S}^{-1}(\mathbf{k})=0\,. \tag{A4}$$

This also yields in general terms $\det\underline{U}^{-1}=0$, as can be proven simply. After elementary matrix manipulations $\underline{S}^{-1}(\mathbf{k})$ can be written as

$$\underline{S}^{-1}=\underline{V}\,\underline{U}^{-1}(\underline{S}^{0})^{-1}\,. \tag{A5}$$

The identity $\det(\underline{AB})=(\det\underline{A})(\det\underline{B})$ yields immediately

$$\det[\underline{S}^{-1}(\mathbf{k})]=\det[\underline{V}(\mathbf{k})]\det[\underline{U}^{-1}(\mathbf{k})]\det[(\underline{S}^{0})^{-1}(\mathbf{k})]=0 \tag{A6}$$

and since $\det\underline{V}\neq 0$ and $\det[(\underline{S}^0)^{-1}]\neq 0$, it follows

$$\det\{[\underline{U}(\mathbf{k})]^{-1}\}=0 \tag{A7}$$

at the critical point and the critical wave vector.

APPENDIX B: MEAN-FIELD THEORY OF SOLVENT: SHIFT OF THE SPINODAL

Equation (60) from the main text can be readily generalized to the case of block copolymers in solution with solvent concentration ϕ_S (playing the role of ϕ_V),

$$\chi_c(\mathbf{k})=\frac{1}{2}\left\{\left[\frac{S^0_{AA}}{\det\underline{S}^0}+\frac{1}{\phi_S}-\chi_{AS}\right]\times\left[\frac{S^0_{BB}}{\det\underline{S}^0}+\frac{1}{\phi_S}-\chi_{BS}\right]\right\}^{1/2}-\left[\frac{1}{\phi_S}-(\chi_{AS}+\chi_{BS})\right]+\frac{S^0_{AB}}{\det\underline{S}^0}\,, \tag{B1}$$

where χ_{AS} and χ_{BS} are the interaction parameters of the species A and B with the solvent. The $\chi_{\sigma\tau}$ are the usual combinations of the potentials $V_{\sigma\tau}$ [see Eq. (54) and [50]]. Vacancies are the special case $\chi_{\sigma\tau}=0$, $\forall\sigma$, $\tau=A,B,V$, and $S=V$.

[1] F. S. Bates, J. H. Rosedale, and G. H. Fredrickson, J. Chem. Phys. **92**, 6255 (1990).
[2] K. Almdal, J. H. Rosedale, F. S. Bates, and G. D. Wignall, Phys. Rev. Lett. **65**, 1112 (1990).
[3] B. Stühn, R. Mutter, and T. Albrecht, Europhys. Lett. **18**, 427 (1992).
[4] B. Stühn and F. Stickel, Macromolecules **25**, 5306 (1992).
[5] B. Stühn, J. Polym. Sci. Polym. Phys. **30**, 1013 (1992).
[6] J. Kanetakis, G. Fytas, F. Kremer, and T. Pakula, Macromolecules **25**, 3484 (1992).
[7] G. Fytas, I. Alig, A. Rizos, J. Kanetakis, F. Kremer, and J. Roovers, J. Polym. Prep. Am. Chem. Soc. Div. Polym. Chem. **33**, 86 (1992).
[8] I. Alig, F. Kremer, G. Fytas, and J. Roovers, Macromolecules **25**, 5277 (1992).
[9] A. Z. Akcasu, M. Benmouna, and H. Benoit, Polymer **27**, 1935 (1986).
[10] G. H. Fredrickson and E. Helfand, J. Chem. Phys. **87**, 697 (1987).
[11] H. Benoit and G. Hadziioanou, Macromolecules **21**, 1449 (1988).
[12] F. S. Bates and G. H. Fredrickson, Annu. Rev. Phys. Chem. **41**, 525 (1990).
[13] R. Borsali and T. A. Vilgis, J. Chem. Phys. **92**, 3610 (1990).
[14] T. A. Vilgis, M. Benmouna, and H. Benoit, Macromolecules **24**, 4482 (1991).
[15] R. Holyst and M. Schick, J. Chem. Phys. **96**, 7728 (1992).
[16] M. Benmouna and Y. Bouayed, Macromolecules **25**, 5319 (1992).
[17] B. Minchau, B. Dünweg, and K. Binder, Polym. Commun. **31**, 8349 (1990).
[18] H. Fried and K. Binder, J. Chem. Phys. **94**, 8349 (1991).
[19] A. Chakrabarti, R. Toral, and J. D. Gunton, Phys. Rev. Lett. **63**, 2661 (1989); Phys. Rev. A **44**, 6503 (1991).
[20] L. Leibler, Macromolecules **13**, 1602 (1980).
[21] S. A. Brazowskii, Zh. Eksp. Teor. Fiz. **68**, 175 (1975) [Sov. Phys. JETP **41**, 85 (1975)].
[22] A. Sariban and K. Binder, J. Chem. Phys. **86**, 5859 (1987); Macromolecules **21**, 711 (1988).
[23] I. Carmesin and K. Kremer, Macromolecules **21**, 2819 (1988).
[24] H. P. Deutsch and K. Binder, J. Chem. Phys. **94**, 2294 (1990).
[25] O. F. Olaj and W. Lantschbauer, Makromol. Chem. Rap. Comm. **3**, 847 (1982).
[26] S. Geyler, T. Pakula, and J. Reiter, J. Chem. Phys. **92**, 2676 (1990).
[27] J. Reiter, Macromolecules **23**, 3811 (1990).
[28] J. Reiter, T. Edling, and T. Pakula, J. Chem. Phys. **93**, 837 (1990).
[29] A. Gauger and T. Pakula, J. Chem. Phys. **98**, 3548 (1993).
[30] A. Gauger, A. Weyersberg, and T. Pakula, Makromol. Chem., Theory Simul. (to be published).
[31] N. Metropolis, A. W. Rosenbluth, M. N. Rosenbluth, A. H. Teller, and E. Teller, J. Chem. Phys. **21**, 1087 (1953).
[32] J. Reiter (unpublished).
[33] S. F. Edwards and M. Muthukumar, J. Chem. Phys. **76**, 2720 (1982).
[34] T. Ohta and A. Nakanishi, J. Phys. A **16**, 4155 (1983).
[35] Y. Oono, Adv. Chem. Phys. **61**, 353 (1985).
[36] J. L. Barrat and G. H. Fredrickson, J. Chem. Phys. **95**, 1281 (1990).
[37] S. F. Edwards, Proc. Phys. Soc. London **88**, 265 (1965).
[38] V. J. Emery, Phys. Rev. B **11**, 239 (1975).
[39] A. Kholodenko and K. Freed, J. Chem. Phys. **78**, 7390 (1993).
[40] J. F. Joanny, L. Leibler, and R. C. Ball, J. Chem. Phys. **81**, 4640 (1984).
[41] J. des Cloizeaux and G. Janninck, *Polymers in Solution* (Clarendon, Oxford, 1991).
[42] T. Ohta and K. Kawasaki, Macromolecules **19**, 2621 (1986).
[43] T. A. Vilgis, and R. Borsali, Macromolecules **23**, 3172 (1990).
[44] M. G. Brereton, and T. A. Vilgis, J. Phys. France **50**, 245 (1989).
[45] H. Hasegawa, T. Hashimoto, H. Kawai, T. P. Lodge, E. J. Amis, L. J. Glinka, and C. C. Han, Macromolecules **18**, 67 (1985).
[46] K. Binder, in *Finite Size Scaling and Numerical Simulations of Statistical Systems,* edited by V. Privman (World Scientific, Singapore, 1990).
[47] M. G. Brereton, T. A. Vilgis, and A. Weyersberg (unpublished).
[48] H. Benoit and M. Benmouna, Macromolecules **17**, 535 (1984).
[49] J. Dudowics and K. F. Freed, Macromolecules **24**, 5076 (1991).
[50] T. A. Vilgis, M. Benmouna, and H. Benoit, Macromolecules **24**, 4482 (1991).
[51] K. W. Kehr, K. Binder, and S. M. Reulein, Phys. Rev. B **39**, 4891 (1989).

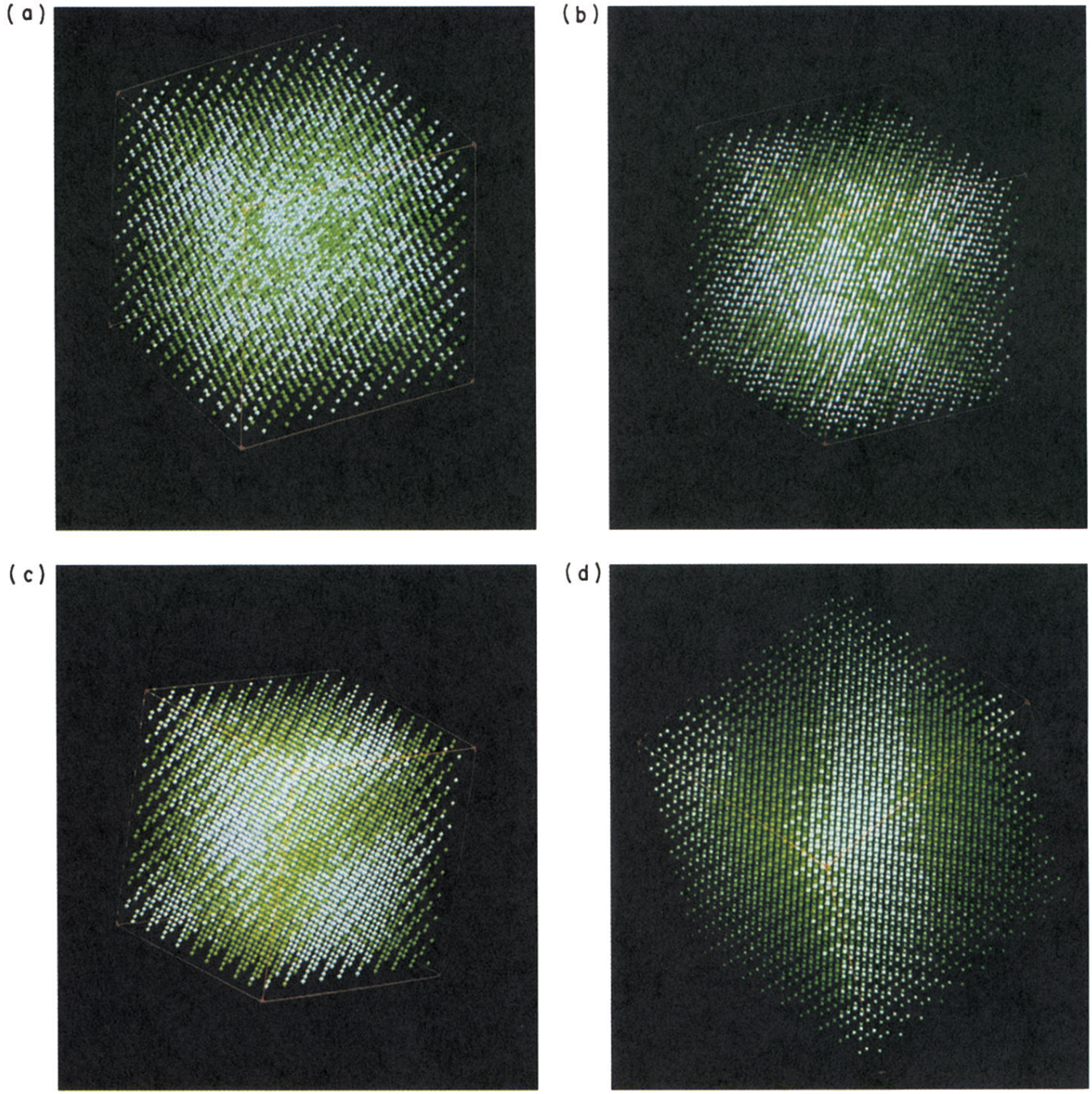

FIG. 9. Snapshots of an $N=20$ diblock copolymer melt at different temperatures. The green and white symbols refer to the different types of monomers, whereas bonds have been omitted for a better overview. The value of $k_B T_c/\varepsilon$ is taken from the specific heat (Fig. 11) for $N=20$. (a) At $k_B T/\varepsilon=20 \gg k_B T_c/\varepsilon$ the melt is homogeneously mixed. (b) Above $k_B T_c/\varepsilon$ ($k_B T/\varepsilon=14$) compositional fluctuations can already be observed. (c) At the critical point of the melt, a lamellar structure arises ($k_B T/\varepsilon \sim 9.0$). (d) A few temperature steps below $k_B T_c/\varepsilon$ ($k_B T/\varepsilon=8$) a clear lamellar structure has been developed.